An Investigation of KS-DFT Electron Densities used in Atoms-in-Molecules Studies of Energetic Molecules

Anthony D. Yau,*,† Edward F. C. Byrd, and Betsy M. Rice

U.S. Army Research Laboratory, Aberdeen Proving Ground, Maryland 21005

Received: February 05, 2009; Revised Manuscript Received: March 16, 2009

The atoms-in-molecules (AIM) theory has been proposed as a method to understand chemical stability through stationary properties of the electron density. To assess the applicability of this method for establishing such correlations with various performance and vulnerability properties of energetic materials, we calculated the Kohn−Sham density functional theory (KS-DFT) wavefunctions and their subsequent AIM data for representative materials, including hexanitrobenzene (HNB), pentaerythritol tetranitrate (PETN), pentanitroaniline (PNA), 1,3,5,7-tetranitro-1,3,5,7-tetrazocine (HMX), ethylenedinitramine (EDNA), 1,1-diamino-2,2-dinitroethylene (FOX-7), 3-nitro-1,2,4-triazol-5-one (NTO), nitroguanidine (NQ), 1,3,5-triamino-2,4,6-trinitrobenzene (TATB), and the TATB dimer using the B3LYP, PBE, and PW91 potentials as well as Hartree−Fock (HF). For the HNB and HMX molecules and the TATB dimer, the number of critical points in the low-density regions of the density gradient vector field varied, sometimes dramatically, with basis set and potential even at their individually optimized geometries. Adding ghost atoms in the low-density regions also affected the existence of critical points. The variation was seen in results generated with three separate AIM software packages, AIMPAC, AIMAll, and InteGriTy. This inconsistency implies that KS-DFT wavefunctions can have significant variation in the topology of the electron density to such an extent that these calculations cannot be used to justify the existence or absence of low-density critical points. Therefore, predictions of the stability of a molecule based solely on properties of low-density bond critical points generated from a single DFT calculation are questionable.

Introduction

In recent years, advances in theoretical models have improved the ability to predict performance properties of energetic materials (EMs).[1,2] Consequently, computational methods allow researchers to screen hypothetical energetic materials and focus synthesis efforts solely on those candidates that display the most promise.[3−6] To date, the theoretical models have concentrated mainly on performance properties such as heats of formation and mass densities.[2,7−11] An equally important property of an EM that has yet to be accurately assessed with theory is its sensitivity to impact.[12−16] In an earlier effort,[17] Rice and Hare explored several functional relations between features of a molecule's electrostatic potential (ESP) mapped onto the $\rho_{0.001}$ isosurface of electron density to an EM's sensitivity to impact, represented by results of drop hammer tests.[18] While only weak correlations between various functions and these features were determined, a striking visual correlation of the ESPs with impact sensitivity was obtained when the values of charge were represented by color. The color mappings imply a direct correlation between the degree of sensitivity and the degree of electron deficiency over covalent bonds within the structure of the sampled explosives. The mappings showed that sensitive explosives had regions of significant electron deficiency localized over covalent bonds of the molecular structures, whereas the insensitive explosives did not. While this study provided a useful qualitative indicator of the degree of sensitivity of EMs, it did not yield a physically meaningful, generally applicable, explanation of the apparent correlation. This led to our interest in further, more rigorous studies into whether other properties of the electronic density could be used to predict impact sensitivity.

Our pursuit of establishing correlations between atoms-in-molecules[19] (AIM) data and sensitivity was fueled by the work of Pinkerton et al., who proposed that the energy required for the shock initiation of an EM could be obtained from rupture of intermolecular "bonds", defined by AIM analyses.[20] Further, they anticipated that the sensitivity of an EM might be related to these intermolecular "bonds" or other AIM properties.[21] Pinkerton et al. computed AIM values for electron densities of EMs using multipole expansions fitted to experimental X-ray diffraction data[20−26] using the XD program[27] for refinement and WinXPRO[28] for the AIM analysis. In addition to this empirical procedure, they also used CRYSTAL98[29] to calculate periodic B3LYP wavefunctions at the experimental geometry and generated AIM data with the TOPOND program.[30] The ability of AIM to probe regions of the electron density and to assign energy values to specific nuclei and intermolecular "bonds" suggests a more theoretically rigorous approach to Rice's earlier effort.

In an exploratory study of selected EMs found in ref 17, we used the AIMPAC software package[31] to calculate AIM properties from a Kohn−Sham (KS) DFT single-determinant wavefunction. For some EMs, however, the number of intra- and intermolecular critical points (CPs) changed across DFT potentials and basis sets. For example, the number of bond/ring CPs for HNB in the regions between the nitro groups ranges from 2 to 12 (Figure 1). Two review articles discuss the application of AIM to charge densities in crystals[33,34] and note some of the inconsistencies in experimental and theoretical

* To whom correspondence should be addressed. E-mail: anthony.yau@arl.army.mil.

† A. D. Yau works for High Performance Technologies, Inc., a contractor with the Army Research Laboratory.

10.1021/jp9010845 CCC: $40.75 © 2009 American Chemical Society
Published on Web 04/10/2009

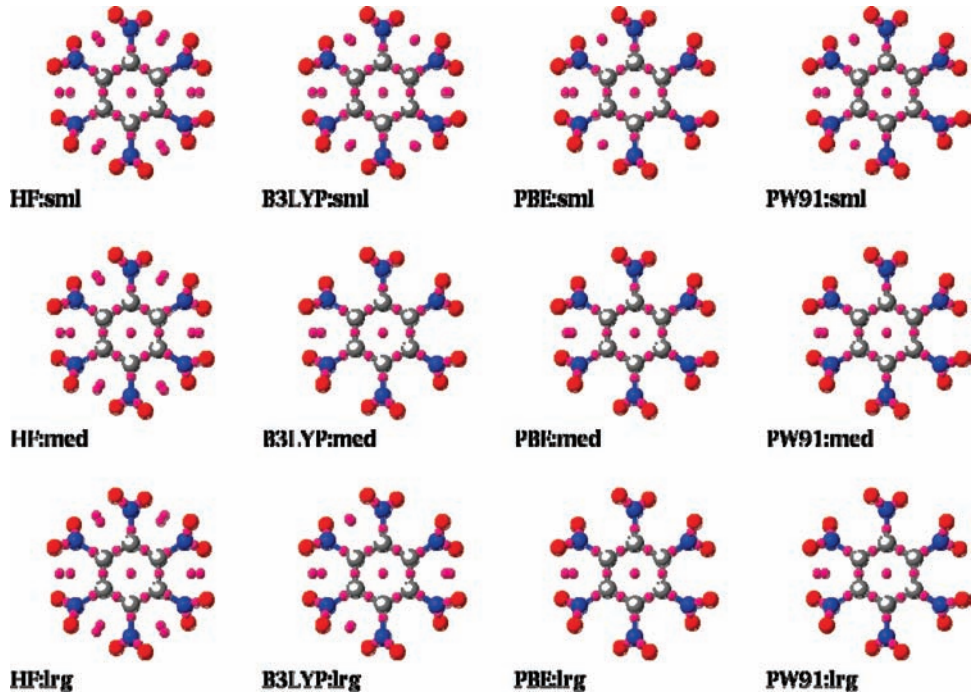

Figure 1. Critical points in the HNB density gradient vector field. The molecular geometry was taken from the experimental crystal structure, and the electron density was computed by GAMESS[32] using the 6-31G*, 6-311++G(2d,2p), and 6-311++G(3df,3pd) basis sets, labeled sml, med, and lrg, respectively. The pink dots are centered on the bond and ring critical points found by the AIMPAC program.

TABLE 1: Selection of Energetic Materials[a]

abbreviation	CSD Refcode	formula	$h_{50\%}$(cm)
HNB	HNOBEN	$C_6N_6O_{12}$	11[b]
PETN	PERYTN12	$C_5H_8N_4O_{12}$	13[c]
PNA	KELZEH	$C_6H_2N_6O_{10}$	22[b]
β-HMX	OCHTET12	$C_4H_8N_8O_8$	29[d]
EDNA	DNEDAM	$C_2H_6N_4O_4$	34[d]
FOX-7	SEDTUQ01	$C_2H_4N_4O_4$	126[e]
α-NTO	QOYJOD06	$C_2H_2N_4O_3$	291[d]
NQ	NTRGUA02	$C_1H_4N_4O_2$	320[c]
TATB	TATNBZ	$C_6H_6N_6O_6$	490[d]

[a] Refcodes are entry identifiers in the Cambridge Structural Database[40] for the experimental structures used in this study. [b] Reference 42. [c] Reference 43. [d] Reference 44. [e] Reference 45. For those systems with more than one Refcode, the experimental structure chosen for the study is that resolved at experimental temperatures closest to 300 K and with the lowest *R* factor.

analyses of electron density.[35−37] The current study is an attempt to determine the source of the inconsistencies in the AIM data for isolated molecules and to evaluate the feasibility of using AIM as a method of modeling the sensitivity in energetic materials.

Methodology

In our exploratory study with AIMPAC, nine compounds, listed in Table 1, were chosen; these span the range of experimental drop weight impact test results, given as $h_{50\%}$ values.[38] The set of molecules explored in this study includes nitroaromatics, nitrate esters, polynitroanilines, nitramines, nitrotriazoles, and nitroalphatics. For all of the molecules in this study, we generated spin-restricted KS-DFT single-determinant wavefunctions using four potentials, nonlocal exact exchange (HF), B3LYP, PBE, and PW91 with three Gaussian basis sets[39] (small) 6-31G*, (medium) 6-311++G(2d,2p), and (large) 6-311++G(3df,3pd). The nuclear positions are consistent with the experimental crystal structures contained in the Cambridge Structural Database[40] and identified by Refcode in Table 1. Unless otherwise noted in the text, the calculations were performed with the March 24, 2007 R1 version of the GAMESS program package,[32] which uses the VWN5 correlation functional in B3LYP rather than the VWN3 functional as found in Gaussian03.[41]

The electron density was converged to 10^{-10} with Fock differencing disabled. The DFT numerical integration used atom-centered polar grids with 36 theta planes, 72 phi planes, and 96 radial shells, and effectively all Fock contributions were included (down to 10^{-15}). Some basis sets had linear dependencies in their symmetry-adapted linear combinations, but the majority of the calculations had overlap eigenvalue thresholds of 10^{-7}. Two-electron integrals were evaluated down to 10^{-20}, and the primitive cutoff was lowered to 10^{-30}. To minimize truncation error in the wavefunction, GAMESS was modified to create a binary wfn file, and the AIMPAC programs were then modified to read in the unformatted data.

The critical point (CP) search program in AIMPAC loops over all sets of nuclei that have one, two, three, or four atoms. In some cases, this CP search algorithm does not find all of the critical points; typically, those cases involve two points (usually a bond/ring pair) that are very close to one another. A more extensive search algorithm for CPs exists in the program AIMAll,[46] a modern descendant of AIMPAC. We examined its exhaustive automated search strategy and subsequently developed a similar strategy that we used in AIMPAC.

Finally, to ensure that any missing CPs were not overlooked due to the line integrator methodologies of AIMPAC and AIMAll, we obtained another CP search program, InteGriTy.[47] Instead of creating the density and its gradient from a wavefunction, InteGriTy uses tricubic Lagrange interpolation of scalars (the density or Laplacian) on a three-dimensional grid. The *cubev* program in AIMPAC was modified to create a binary data file for use with InteGriTy, and the electron density was sampled at 0.05 Å intervals. For the PNA molecule, we had to

TABLE 2: Number of Critical Points Found in a Series of Molecules That Form Energetic Crystals[a]

molecule	basis	potential	CPs	NCP	BCP	RCP	CCP	χ
PETN	all	all	57	29	28	0	0	1
PNA	all	all	61	24	30	7	0	1
EDNA	all	all	31	16	15	0	0	1
FOX-7	all	all	33	14	16	3	0	1
NTO	all	all	23	11	11	1	0	1
NQ	all	all	23	11	11	1	0	1
TATB	all	all	61	24	30	7	0	1
HNB	small	HF	61	24	30	7	0	1
		B3LYP	61	24	30	7	0	1
		PBE	55	24	27	4	0	1
		PW91	55	24	27	4	0	1
	medium	HF	61	24	30	7	0	1
		B3LYP	51	24	25	2	0	1
		PBE	51	24	25	2	0	1
		PW91	51	24	25	2	0	1
	large	HF	61	24	30	7	0	1
		B3LYP	57	24	28	5	0	1
		PBE	51	24	25	2	0	1
		PW91	51	24	25	2	0	1
HMX	small	HF	63	28	31	4	0	1
		B3LYP	63	28	31	4	0	1
		PBE	63	28	31	4	0	1
		PW91	63	28	31	4	0	1
	medium	HF	63	28	31	4	0	1
		B3LYP	59	28	29	2	0	1
		PBE	59	28	29	2	0	1
		PW91	59	28	29	2	0	1
	large	HF	63	28	31	4	0	1
		B3LYP	63	28	31	4	0	1
		PBE	59	28	29	2	0	1
		PW91	59	28	29	2	0	1
TATB dimer	small	HF	143	48	69	24	2	1
		B3LYP	135	48	65	20	2	1
		PBE	135	48	65	20	2	1
		PW91	135	48	65	20	2	1
	medium	HF	147	48	71	26	2	1
		B3LYP	145	48	68	25	4	1
		PBE	141	48	66	23	4	1
		PW91	141	48	66	23	4	1
	large	HF	147	48	71	26	2	1
		B3LYP	147	48	69	26	4	1
		PBE	141	48	66	23	4	1
		PW91	141	48	66	23	4	1

[a] Basis sets and potentials referred to as "all" apply only to those used in this study.

reduce the spacing to 0.04 Å because InteGriTy did not identify two high-density BCPs using the default grid.

Results

Table 2 lists the number and type of critical points that all three programs found for the surveyed species. For all but two of the molecules, the choice of basis set and DFT potential did not change the number or types of critical points. For the HNB and HMX molecules, however, the density has different numbers of critical points depending on which basis set and which DFT potential are used.

One method for verifying if all CPs have been found for a given electronic density is to calculate the Euler characteristic χ from the Poincaré−Hopf relationship (a necessary but insufficient condition of verification)[48]

$$\chi = n - b + r - c \quad (1)$$

for which n, b, r, and c refer to the number of nuclear, bond, ring, and cage critical points, respectively. For nonperiodic systems, χ should be 1 if a consistent set of CPs is found.[49−51] However, having a consistent set does not guarantee that the global set of CPs is found; it only suggests that all of the CPs that are found are matched appropriately. For example, χ can remain 1 if a pair of bond and ring CPs is removed from the previously consistent set.

TABLE 3: Number of Outer Bond/Ring CP Pairs in HNB and HMX

basis set	HF	B3LYP	PBE	PW91
		HNB		
small	6	6	3	3
medium	6	1	1	1
large	6	4	1	1
		HMX		
small	2	2	2	2
medium	2	0	0	0
large	2	2	0	0

Table 3 lists the number of bond/ring CP pairs found in the outer five- and six-member rings of HNB (Figure 1) and HMX. We note that these outer bond CPs are in low-density regions, and the values of ρ at these BCPs are an order of magnitude smaller than the values calculated for the traditional "bonding" intramolecular BCPs.

To study the variability in CP pairs when the basis set or DFT potential is changed, we examined the search paths in the outer ring of HMX for B3LYP in the medium basis set, 6-311++G(2d,2p). This combination of method and basis set does not have the two outer CP pairs and appears to be an outlier for the theory in Table 2 (more readily apparent in Table 3). Figure 2a highlights the CPs found in the other methods, and Figure 2b traces the search paths that AIMPAC follows in this region of the B3LYP/6-311++G(2d,2p) (B3LYP/medium) electron density. Clearly, the stepping algorithm converges to the correct vicinity but does not arrive at a point with near-zero gradient (10^{-10} e/Å) for this method and basis set.

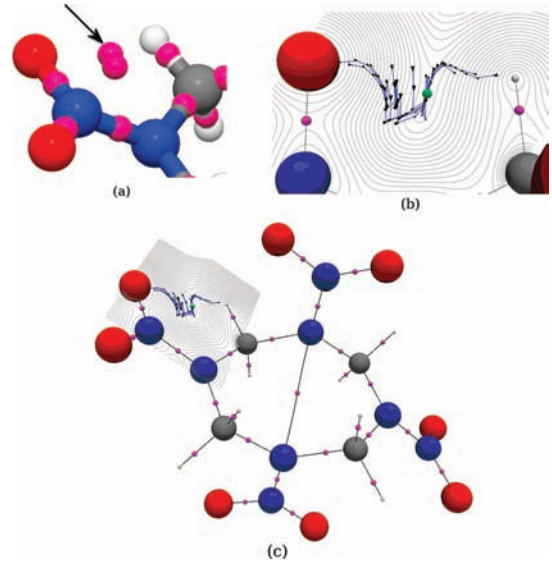

Figure 2. AIMPAC search paths in HMX in the medium basis set. Image (a) points to the bond and ring critical points in the HF density between the NO_2 oxygen and the CH_2 hydrogen. Image (b) shows contour lines and the search paths in the B3LYP density that AIMPAC follows. The green dot in (b) is the location of the BCP as found in the HF density and not in the B3LYP density. Image (c) shows the complete molecule, rotated slightly from the orientation in (b). There are two ring CPs on either side of the bond CP in the center of the molecule, but they are not shown in (c).

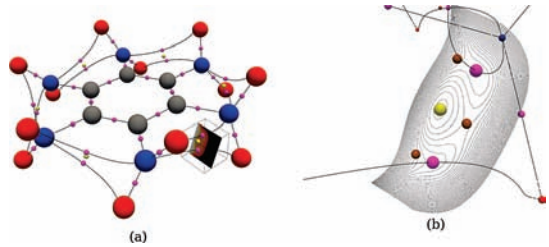

Figure 3. Critical points of individually optimized HNB molecules. The results in the row of medium basis set calculations are consistent, and the results in the column of PBE calculations are consistent.

TABLE 4: Total Number of Critical Points Found at Individually Optimized Ground-State Geometries of HNB[a]

basis set	HF	B3LYP	PBE	PW91
small	61	85 (82)	49	61
medium	49	49	49	49
large	61	49	49	49

[a] The B3LYP/small value should be 85 due to point group symmetry, although AIMPAC only finds 82, which has an Euler characteristic of −2.

The bond critical point is 0.94 Å from the hydrogen nucleus and 1.28 Å from the oxygen nucleus. In the 6-311++G(2d,2p) basis set, the broadest s functions for hydrogen and oxygen have exponents of 0.036 and 0.0845, respectively. The values of these gaussians at the BCP are 89% of the hydrogen peak and 61% of the oxygen peak; therefore, the coverage of the basis set should be sufficient to describe the missing CP. However, in order to influence the density at the "missing" BCP location, we placed basis functions from hydrogen (ghost atoms) at the missing critical point and computed a new set of KS orbitals. This procedure is usually reserved for correcting the basis set superposition error;[52] however, it guarantees that the wavefunction could relax into the gap. Surprisingly, HMX/B3LYP in the medium basis set with ghost atoms found both pairs of outer CPs. This result challenges the notion that the inner volume of a molecule is correctly described by a "fairly diffuse" basis set and raises the specter of having to fill the space that the molecule occupies with ghost atoms to properly study the electronic topology. Adding ghost atoms might seem obvious for this molecule when we know where missing CPs should be, but this action is not feasible in a general application for all molecules and all basis sets.

A recurring source of confusion over the application of AIM theory concerns net forces on the nuclei, that is, the geometry must be at electrostatic equilibrium.[25,34,53] As all of the aforementioned calculations were performed at geometries extracted from the experimental crystal structure, we optimized the geometry of HNB using each DFT potential in each basis set (shown in Figure 3 and summarized in Table 4) to test whether there would be any effect on the results. Even at optimized geometries, the HF medium basis set topology differs from the HF small and large basis set topologies. The B3LYP and PW91 small basis set topologies differ from their corresponding medium and large basis set topologies, although this is not unexpected. We see only two trends, none of the medium basis results have outer CP pairs and none of the PBE results have outer CP pairs. Finally, we optimized HMX in each basis set with all 4 DFT potentials, and all 12 calculations yield 2 CP pairs in the outer rings. Therefore, while optimizing the geometry corrected the original HMX inconsistencies, HNB still did not produce a consistent set of CPs across methods or basis sets even at the optimized equilibrium geometries.

The most intriguing and most untrustworthy calculation of the series is the B3LYP small basis set calculation at the optimized HNB geometry. The outer rings each have clusters of six CPs, two bonds, three rings, and one cage critical point. These critical points were found regardless of whether AIMPAC or InteGriTy was used. The computational procedure was repeated with Gaussian03, which also shows these CP clusters, and unlike the integral settings used in GAMESS, the G03 run used default settings except for SCF convergence (10^{-7}) and integration grid granularity (Grid = −96036). Therefore, we believe these results to be a specific consequence of the molecule and basis set. Figure 4 shows the bond paths and highlights one of the clusters. We placed ghost hydrogens at the CCPs and reoptimized the geometry, and the final AIM analysis yielded simple bond/ring CP pairs in the outer rings for 61 total CPs, similar to the HF/small result.

In addition to the single-molecule calculations, we have also examined the intermolecular bond paths in a particular TATB dimer conformation using the same set of methods and basis sets. The TATB crystal is aligned in graphite-like sheets with very stable hydrogen bonds between monomers in the same sheet; however, when viewing nearest-neighbor monomers normal to their sheets (Figure 5a), we can see that identifying possible bond paths is far less intuitive. Table 5 lists the number of each type of CP found between the monomers. When projected onto a 2D plane, the bond, ring, and cage critical points have signature values of (2,−2), (2,0), and (2,+2), respectively. The 2D Euler characteristic becomes $b - r + c$, which should equal 1 for an open system, and indeed, all of the potentials and basis sets provide a consistent set of CPs. The only BCPs that appear in all 12 calculations are those that connect the amine nitrogens. With the medium and large basis sets, bond paths are seen between pairs of oxygen atoms. Figure 5b illustrates the two $N_{amine}-N_{amine}$ and two O−O intermolecular bond paths from the PBE/medium density, which also has two $C-N_{nitro}$ bond paths. As seen with the monomers, the number of different types of CPs varies with basis set and method. This variability, along with the necessity to use ghost atoms, calls into question the suitability of a single calculation to qualify, much less quantify, properties at the critical points in the electron density.

Previously, AIM theory has been used to qualify the stability of chemical structures based on the presence of inter- and intramolecular bond critical points. At electrostatic equilibrium, the value of the electronic potential energy at the bond critical point is suspected to be a measure of the bond stabilization energy. However, given the typical basis sets and DFT potentials in use today, low-density BCPs resulting from these calculations, especially those found in weak intra- and intermolecular bonding, should be considered very carefully when used to analyze structural stability. Furthermore, simply increasing the size and number of functions centered on each atom is no guarantee that the description of the electron density will improve with these commonly used DFT potentials. We hypothesize that the magnitude and quality of the density in these low-density regions is within the uncertainty of these potentials, and therefore, any claims as to the exact location or even existence of a critical point (and its corresponding properties) must be called into question. In a subsequent study, we intend to calculate the second-order many-body perturbation theory, MBPT(2), and coupled-cluster singles and doubles (CCSD) density matrices for some of the "troublesome" compounds presented here. While very computationally demanding, these calculations should provide a definitive picture of whether ab initio quantum chemistry calculations can provide

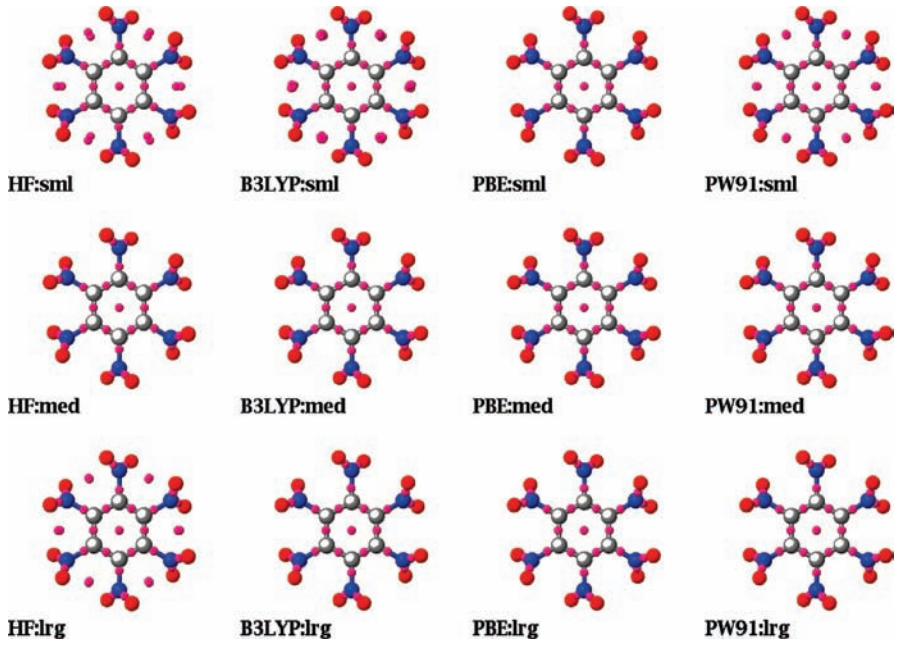

Figure 4. CP data for the optimized HNB geometry with B3LYP/6-31G*. Image (a) shows the entire molecule with a colored plane slicing through the cage and bond CPs. Image (b) shows a magnified view of the plane with isodensity lines instead of color mapping. The blue nitrogen and red oxygen spheres have been severely reduced in size, so that they do not eclipse the area of interest. Bond CPs are pink, ring CPs are brown (not shown in (a)), and the cage CP is yellow. The clusters of CPs are not seen if ghost hydrogens are placed at the cage CPs.

TABLE 5: Number of Intermolecular Critical Points Found at Experimentally Determined TATB Dimer Geometry in the Stacked Configuration Shown in Figure 5[a]

basis set	HF			B3LYP			PBE			PW91		
	BCP	RCP	CCP	BCP	RCP	CCP	BCP	RCP	CCP	BCP	RCP	CCP
small	9	10	2	5	6	2	5	6	2	5	6	2
medium	11	12	2	8	11	4	6	9	4	6	9	4
large	11	12	2	9	12	4	6	9	4	6	9	4

[a] Values correspond to the number of intermolecular bond (BCP), ring (RCP), and cage CPs (CCP), respectively.

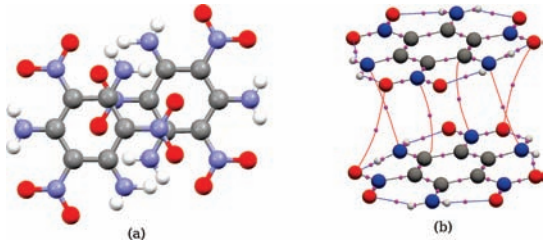

Figure 5. Adjacent TATB molecules from neighboring sheets in the crystal. Image (a) shows the orientation of the chosen dimer, viewed perpendicular to the plane. Image (b) traces the bond paths in the PBE/medium density, with intermolecular bond paths in red.

sufficiently accurate electron densities for use in an atoms-in-molecules analysis of low-density regions.

Conclusion

In this work, we applied the atom-in-molecules theory to a series of energetic molecules in an attempt to establish a correlation between properties of a molecule's electron density with measured impact sensitivities. GAMESS calculations were configured to minimize numerical errors in the DFT wavefunction so that precise electron densities could be generated for use in atoms-in-molecules analyses, including modifications allowing the wavefunction to be written in binary format for postprocessing in order to remove any truncation errors. Even with these precautions, the AIM results for HMX and HNB, along with the results for the TATB dimer, are entirely inconsistent, displaying a variable number of critical points depending on the choice of DFT method and basis set. For all other single molecules studied herein (PETN, PNA, EDNA, FOX-7, NTO, NQ, and TATB) the number of critical points does not change, regardless of basis set or DFT potential. With the differences in numbers of CPs seen in HMX, HNB, and the TATB dimer, trusting an arbitrary AIM analysis for any sufficiently complex molecule or crystal would be difficult, especially when the aforementioned computational precautions may be overlooked or deemed unnecessary. When performing similar AIM analyses to those presented here, care should be taken when assigning significance to the existence or nonexistence of CPs in molecular geometries since a slight variation in nuclear coordinates, basis set, or computational method can drastically alter the results. For molecules that form crystals of energetic materials, KS-DFT wavefunctions can have significant variation in the topology of the electron density to such an extent that these calculations cannot be used to justify the existence or absence of critical points, especially in the regions of low density; therefore, these calculations currently cannot be used to establish correlations between AIM results and impact sensitivity of energetic materials.

Acknowledgment. We extend thanks to the U.S. Department of Defense High Performance Computing Modernization Program for computational resources and support of those resources through the User Productivity Enhancement and Technology Transfer Program (PET), to the U.S. Office of Naval Research

for supporting the research and development of modeling and simulation capabilities of energetic materials, and to the Army Research Laboratory Computer Information Sciences Directorate for supporting the scientific visualization software. We warmly thank R. F. W. Bader for enlightening discussions in the early phases of this work and P. Rabiller, T. A. Keith, and C. Gatti for sharing copies of their AIM programs. We also recognize M. Schmidt for guidance in the use and modification of the GAMESS program.

References and Notes

(1) Rice, B. M. In *Overviews of Recent Research on Energetic Materials*; Shaw, R. W., Brill, T. B., Thompson, D. L., Eds.; Advanced Series in Physical Chemistry 16; World Scientific Publishing Co.: Singapore, 2005; pp 335−368.

(2) *High Energy Density Materials*; Klapötke, T. M., Ed.; Structure and Bonding 125; Springer: Berlin, Germany, 2007.

(3) Lommerse, J. P. M.; Motherwell, W. D. S.; Ammon, H. L.; Dunitz, J. D.; Gavezzotti, A.; Hofmann, D. W. M.; Leusen, F. J. J.; Mooij, W. T. M.; Price, S. L.; Schweizer, B.; Schmidt, M. U.; van Eijck, B. P.; Verwer, P.; Williams, D. E. *Acta Crystallogr., Sect. B* **2000**, *56*, 697.

(4) Day, G. M.; Motherwell, W. D. S.; Ammon, H. L.; Boerrigter, S. X. M.; Della Valle, R. G.; Venuti, E.; Dzyabchenko, A.; Dunitz, J. D.; Schweizer, B.; van Eijck, B. P.; Erk, P.; Facelli, J. C.; Bazterra, V. E.; Ferraro, M. B.; Hofmann, D. W. M.; Leusen, F. J. J.; Liang, C.; Pantelides, C. C.; Karamertzanis, P. G.; Price, S. L.; Lewis, T. C.; Nowell, H.; Torrisi, A.; Scheraga, H. A.; Arnautova, Y. A.; Schmidt, M. U.; Verwer, P. *Acta Crystallogr., Sect. B* **2005**, *61*, 511.

(5) Singh, R. P.; Verma, R. D.; Meshri, D. T.; Shreeve, J. M. *Angew. Chem., Int. Ed.* **2006**, *45*, 3584, and references therein.

(6) Gao, H.; Ye, C.; Piekarski, C. M.; Shreeve, J. M. *J. Phys. Chem. C* **2007**, *111*, 10718.

(7) Fried, L. E.; Manaa, M. R.; Pagoria, P. F.; Simpson, R. L. *Annu. Rev. Mater. Res.* **2001**, *31*, 291.

(8) Byrd, E. F. C.; Rice, B. M. *J. Phys. Chem. A* **2006**, *110*, 1005.

(9) Gutowski, K. E.; Rogers, R. D.; Dixon, D. A. *J. Phys. Chem. B* **2007**, *111*, 4788.

(10) Rice, B. M.; Hare, J. J.; Byrd, E. F. C. *J. Phys. Chem. A* **2007**, *111*, 10874.

(11) Byrd, E. F. C.; Rice, B. M. *J. Phys. Chem. A* **2009**, *113*, 345.

(12) Politzer, P.; Murray, J. S.; Lane, P.; Sjoberg, P.; Adolph, H. G. *Chem. Phys. Lett.* **1991**, *181*, 78.

(13) Politzer, P.; Murray, J. S. *Mol. Phys.* **1995**, *86*, 251.

(14) Murray, J. S.; Lane, P.; Politzer, P. *Mol. Phys.* **1998**, *93*, 187.

(15) Politzer, P.; Murray, J. S. In *Energetic Materials: Part 2, Detonation, Combustion*; Politzer, P., Murray, J. S., Eds; Theoretical and Computational Chemistry 13; Elsevier: Amsterdam, The Netherlands, 2003; pp 5−23.

(16) Murray, J. S.; Concha, M. C.; Politzer, P. *Mol. Phys.* **2009**, *107*, 89.

(17) Rice, B. M.; Hare, J. J. *J. Phys. Chem. A* **2002**, *106*, 1770.

(18) Kamlet, M. J. In Proceedings of the International Symposium on Detonation (6th), Coronado, CA, Aug 24−27, 1976; Edwards, D. J., Jacobs, S. J., Eds.; Office of Naval Research, Department of the Navy: Arlington, VA, 1977; p 312.

(19) Bader, R. F. W. *Atoms in Molecules - A Quantum Theory*; Oxford University Press: Oxford, U.K., 1990.

(20) Zhurova, E. A.; Stash, A. I.; Tsirelson, V. G.; Zhurov, V. V.; Bartashevich, E. V.; Potemkin, V. A.; Pinkerton, A. A. *J. Am. Chem. Soc.* **2006**, *128*, 14728.

(21) Zhurova, E. A.; Zhurov, V. V.; Pinkerton, A. A. *J. Am. Chem. Soc.* **2007**, *129*, 13887.

(22) Zhurova, E. A.; Martin, A.; Pinkerton, A. A. *J. Am. Chem. Soc.* **2002**, *124*, 8741.

(23) Ritchie, J. P.; Zhurova, E. A.; Martin, A.; Pinkerton, A. A. *J. Phys. Chem. B* **2003**, *107*, 14576.

(24) Zhurova, E. A.; Tsirelson, V. G.; Stash, A. I.; Yakovlev, M. V.; Pinkerton, A. A. *J. Phys. Chem. B* **2004**, *108*, 20173.

(25) Zhurova, E. A.; Tsirelson, V. G.; Zhurov, V. V.; Stash, A. I.; Pinkerton, A. A. *Acta Crystallogr., Sect. B* **2006**, *62*, 513.

(26) Chen, Y.-S.; Stash, A. I.; Pinkerton, A. A. *Acta Crystallogr., Sect. B* **2007**, *63*, 309.

(27) Volkov, A.; Macchi, P.; Farrugia, L. J.; Gatti, C.; Mallinson, P.; Richter, T.; Koritsanszky, T. XD2006. http://xd.chem.buffalo.edu (accessed February 2009).

(28) Stash, A.; Tsirelson, V. *J. Appl. Crystallogr.* **2002**, *35*, 371.

(29) Saunders, V. R.; Dovesi, R.; Roetti, C.; Causa, M.; Harrison, N. M.; Orlando, R.; Zicovich-Wilson, C. M. *CRYSTAL98 User's Manual*; University of Torino: Torino, Italy, 1998.

(30) Gatti, C. *TOPOND 98 User's Manual*; CNR-ISTM: Milano, Italy, 1999.

(31) Bader, R. F. W. AIMPAC, online. http://www.chemistry.mcmaster.ca/aimpac/ (accessed February 2009).

(32) Schmidt, M. W.; Baldridge, K. K.; Boatz, J. A.; Elbert, S. T.; Gordon, M. S.; Jensen, J. H.; Koseki, S.; Matsunaga, N.; Nguyen, K. A.; Su, S. J.; Windus, T. L.; Dupuis, M.; Montgomery, J. A. *J. Comput. Chem.* **1993**, *14*, 1347.

(33) Koritsanszky, T. S.; Coppens, P. *Chem. Rev.* **2001**, *101*, 1583.

(34) Gatti, C. *Z. Kristallogr.* **2005**, *220*, 399.

(35) Volkov, A.; Abramov, Y.; Coppens, P.; Gatti, C. *Acta Crystallogr., Sect. A* **2000**, *56*, 332.

(36) Coppens, P.; Volkov, A. *Acta Crystallogr., Sect. A* **2004**, *60*, 357.

(37) Destro, R.; Loconte, L.; Lo Presti, L.; Roversi, P.; Soave, R. *Acta Crystallogr., Sect. A* **2004**, *60*, 365.

(38) Note: drop weight impact tests typically involve dropping a 2.5 kg weight from various heights onto a striker plate, beneath which are milligram quantities of an explosive sample on a flat tool steel anvil. The $h_{50\%}$ value is the height at which 50% of the tests result in a reaction, where reaction is indicated by sound, small, or visual inspection of the sample. The smaller the $h_{50\%}$ value, the more sensitive the compound.

(39) (a) Krishnan, R.; Binkley, J. S.; Seeger, R.; Pople, J. A. *J. Chem. Phys.* **1980**, *72*, 650. (b) Frisch, M. J.; Pople, J. A.; Binkley, J. S. *J. Chem. Phys.* **1984**, *80*, 3265. (c) Clark, T.; Chandrasekhar, J.; Schleyer, P. v. R. *J. Comput. Chem.* **1983**, *4*, 294.

(40) (a) Allen, F. H. *Acta Crystallogr., Sect. B* **2002**, *58*, 380. (b) Bruno, I. J.; Cole, J. C.; Edgington, P. R.; Kessler, M.; Macrae, C. F.; McCabe, P.; Pearson, J.; Taylor, R. *Acta Crystallogr., Sect. B* **2002**, *58*, 389.

(41) Frisch, M. J.; Trucks, G. W.; Schlegel, H. B.; Scuseria, G. E.; Robb, M. A.; Cheeseman, J. R.; Montgomery, J. A., Jr.; Vreven, T.; Kudin, K. N.; Burant, J. C.; Millam, J. M.; Iyengar, S. S.; Tomasi, J.; Barone, V.; Mennucci, B.; Cossi, M.; Scalmani, G.; Rega, N.; Petersson, G. A.; Nakatsuji, H.; Hada, M.; Ehara, M.; Toyota, K.; Fukuda, R.; Hasegawa, J.; Ishida, M.; Nakajima, T.; Honda, Y.; Kitao, O.; Nakai, H.; Klene, M.; Li, X.; Knox, J. E.; Hratchian, H. P.; Cross, J. B.; Bakken, V.; Adamo, C.; Jaramillo, J.; Gomperts, R.; Stratmann, R. E.; Yazyev, O.; Austin, A. J.; Cammi, R.; Pomelli, C.; Ochterski, J. W.; Ayala, P. Y.; Morokuma, K.; Voth, G. A.; Salvador, P.; Dannenberg, J. J.; Zakrzewski, V. G.; Dapprich, S.; Daniels, A. D.; Strain, M. C.; Farkas, O.; Malick, D. K.; Rabuck, A. D.; Raghavachari, K.; Foresman, J. B.; Ortiz, J. V.; Cui, Q.; Baboul, A. G.; Clifford, S.; Cioslowski, J.; Stefanov, B. B.; Liu, G.; Liashenko, A.; Piskorz, P.; Komaromi, I.; Martin, R. L.; Fox, D. J.; Keith, T.; Al-Laham, M. A.; Peng, C. Y.; Nanayakkara, A.; Challacombe, M.; Gill, P. M. W.; Johnson, B.; Chen, W.; Wong, M. W.; Gonzalez, C.; Pople, J. A. *Gaussian 03*, revision C.02; Gaussian, Inc.: Wallingford, CT, 2004.

(42) Wilson, W. S.; Bliss, D. E.; Christian, S. L.; Knight, D. J. *Explosive Properties of Polynitroaromatic*, NWC/TP-7073; Naval Weapons Center: China Lake, CA, 1990.

(43) Hall, T. N.; Holden, J. R. *Navy Explosives Handbook*, NSWC/MP-88-116; Naval Surface Warfare Center: Dahlgren, VA, 1988.

(44) Storm, C. B.; Stine, J. R.; Kramer, J. F. In *Chemistry and Physics of Energetic Materials*; Bulusu, S. N., Ed.; Kluwer Academic Publishers: Dordrecht, The Netherlands, 1990; pp 605−639.

(45) Östmark, H.; Langlet, A.; Bergman, H.; Wingborg, N.; Wellmar, U.; Bemm, U. In Proceedings of the International Symposium on Detonation (11th), Snowmass, Colorado, Aug 30−Sept 4, 1998; Office of Naval Research, Department of the Navy: Arlington, VA, 1978; p 807.

(46) Keith, T. A. AIMAll, online, version 08.01.25. http://aim.tkgristmill.com/ (accessed February 2009).

(47) Katan, C.; Rabiller, P.; Lecomte, C.; Guezo, M.; Oison, V.; Souhassou, M. *J. Appl. Crystallogr.* **2003**, *36*, 65.

(48) Hopf, H. *Math. Ann.* **1926**, *96*, 255.

(49) Leboeuf, M.; Köster, A. M.; Jug, K.; Salahub, D. R. *J. Chem. Phys.* **1999**, *111*, 4893.

(50) Balanarayan, P.; Gadre, S. R. *J. Chem. Phys.* **2003**, *119*, 5037.

(51) Castillo, N.; Matta, C. F.; Boyd, R. J. *Chem. Phys. Lett.* **2005**, *409*, 265.

(52) (a) Boys, S. F.; Bernardi, F. *Mol. Phys.* **1970**, *19*, 553. (b) Jansen, H. B.; Ros, P. *Chem. Phys. Lett.* **1969**, *3*, 140.

(53) Bader, R. F. W. *J. Phys. Chem. A* **1998**, *102*, 7314.

JP9010845